



Research Paper

Prediction of Interface Shear Strength of Heat Damaged Shear-keys using Nonlinear Finite Element Analysis

Rajai Z. Al-Rousan^{ORCID}, Bara'a R. Alnemrawi^{ORCID}

Department of Civil Engineering, Jordan University of Science and Technology, Irbid, 22110, Jordan, Email: rzalrousan@just.edu.jo (R.Z.A.); bralnemrawi19@eng.just.edu.jo (B.R.A.)

Received February 10 2023; Revised April 09 2023; Accepted for publication April 10 2023.

Corresponding author: R.Z. Al-Rousan (rzalrousan@just.edu.jo)

© 2023 Published by Shahid Chamran University of Ahvaz

Abstract. Push-off samples are simulated using nonlinear finite element analysis (NLFEA) to evaluate the effects of increased temperatures on the interface shear strength. Firstly, a control shear-key model is created, calibrated, and confirmed against independently published experimental data. Twenty-four NLFEA models are then created with different variables, including temperature (23°C (Room Temperature), 250°C (Raised temperature), 500°C, and 750°C and the number of steel stirrups (none, 1, 2, 3, 4, and 5). The NLFEA results demonstrate that the decreased fracture opening and slide in the damaged shear keys compared to the intact control sample represent the amazing effect of the number of steel stirrups. In addition, it has been revealed that the longitudinal shear force and slide, mode of failure, rigidity, and toughness are all significantly impacted by the degree of heat damage. In particular, a simplified approach is proposed for calculating the shear strength of push-off samples subjected to higher temperatures.

Keywords: Elevated, Temperature, Shear-key, Push-off, NLFEA, Stirrups.

1. Introduction

Concrete shear failure is a premature, brittle failure that leads to the progressive collapse of the entire structure. In most cases, severe cracking emerges, and propagation takes place immediately. However, as it directly impacts its load-carrying capacity and overall performance, the crack's capacity to sustain shear stresses is essential. Consequently, it is important to understand the principles of shear transmission utilizing various experimental and analytical techniques [1-3]. Assuming that loading is carried by shear at the contact area between the two shear interfaces, the shear-friction theory is a well-known theory investigating the shear behavior at the concrete-concrete interface [4]. Researchers currently use this theory to investigate how shear stress is transferred between two concrete contacts. The application of this theory was further expanded to examine the effects of additional parameters, such as aggregate restriction, adhesive composition, aggregate interlock, and dowel action [5, 6]. Initially, the evaluated RC structural members were designed per code requirements. Moreover, small, inexpensively manufactured, monitored, and highly controlled models that simultaneously measure shear strength and stiffness are necessary to evaluate the shear behavior thoroughly.

The transmission of shear loads through shear planes is the primary factor influencing the efficiency of monolithic concrete joints and interfaces. These are interface bridge deck, girder, and shear wall construction joints. Precast Reinforced Concrete (RC) beams constructed in the workplace have become popular due to the requirement to build reinforced concrete bridges quickly without disturbing traffic or railroad tracks before the concrete hardens, which takes time [7]. The connections with interlocked shear keys which connect these precast concrete beam segments can be used as dry or with a bonding agent [8, 9]. Shear failure is acknowledged as one of the most serious problems requiring more consideration throughout RC structure analysis and design stages [10-12]. Increased traffic volume, exposure to adverse weather, increased permissible stress at service loads, and greater truck loads all have the potential to diminish the integral action between cast-in-situ slabs and precast prestressed concrete girders in composite concrete bridges, increasing the demand for upgrading the joint against shear stresses which could be provided in terms of stirrups [13].

Moreover, the effect of steel stiffeners has been addressed using finite element modeling in the work of Kucharski et al. [14], while the shear band propagation has been examined by Balokhonov et al. [15] using the mesoscopic and the finite element difference approaches. In addition, the concrete and steel withstand shear at an interface. Joints in concrete and their structural effectiveness have been the subject of several analytical and experimental studies, indicating this topic's importance in the concrete mechanics' field. The key factors investigated were the compressive strength of the concrete, the normal stress throughout the interface, the kind of interface, the grade of steel used across the interface, the diameter of the bars, and the various steel layouts given across the interface. A study by Kahn and Mitchell [16] investigated push-off samples of concrete. The equation provided in ACI-318 was found to be a conservative estimate of high-strength concrete interface shear capability. Similarly, a shear capacity equation was proposed. Pre-cracked push-off samples of concrete with strengths between 40.2 and 106.4 MPa were tested by Mansur



et al. [17]. The frictional coefficient at the shear-key interface was shown to be independent of the strength of the concrete material representing the adequacy of assuming a rough interface, following statistical analysis of 154 crack samples. An equation for pre-cracked concrete interface shear capacity was also developed.

It has been demonstrated that high-temperature levels affect the shear capacity of concrete material. Other researchers [18, 19] investigated the effects of high-yield strengthening steel on concrete surfaces and the shear capacity of lightweight materials by contrasting cold-jointed models with rough and smooth surfaces. Despite findings demonstrating a relationship between reinforcement ratio and shear capacity, yield strength of reinforcement was independent of this attribute. Results showed that the unit weight of concrete had no noticeable effect on the shear capabilities of cold-jointed models. It had been demonstrated that the compressive strength of concrete governed the shear capacity of reinforced cold joints. Concrete's compressive strength and surface integrity have almost no effect on the post-ultimate residual capacity. The high-temperature impacts on the shear capacity of reinforcing concrete interfaces cast with concrete of varied compressive strengths were examined by Xiao et al. [20]. The findings showed that samples cast with higher compressive strength concrete showed a more significant shear capacity drop after exposure to high temperatures. A study on the shear strength of self-compacting concrete was carried out by Rahal et al. [21]. They investigated the effects of steel ratio and concrete strength on the performance of RC structures. Interface shear capacity can be significantly improved by significantly increasing the concrete strength and interface steel.

Concrete has considerable chemical and physical modifications when exposed to high temperatures. The cement pastes and aggregates undergo different internal temperatures due to the difference in their specific heat factors. At temperatures above 100 °C, the interfacial transition zone tends to crack, which weakens the concrete by reducing the bonding force between the cement paste and the aggregates. C-S-H gel begins to dissolve at temperatures over 600 °C, greatly lowering the strength of concrete. CaCO₃ decomposes into CaO and CO₂ around 800 °C, lowering the strength of concrete by 70% to 80% [22]. Ahmed et al. [23] examined the behavior of concrete strength under elevated temperatures and found that heating concrete up to 250 and 500 °C will have little impact on the concrete joint's maximum shear strength and failure loads. The shear strength of concrete joints reduced as the temperature increased, and the ability of concrete joints to withstand ultimate shear after being heated was unaffected. Realistic and conservative shear capacity estimations for reinforcing concrete surfaces exposed to higher temperatures may be obtained using a shear capacity model for air temperatures that considers the residual properties of concrete and steel [24]. Push-off type models were utilized in the tests conducted by Ahmad et al. [25, 26]. Concrete samples of 40 MPa were heated to 350, 550, and 750 °C in an electric oven, and the heated samples were left outside to cool to normal room temperature. Results from both cold and heated models demonstrated that when exposed to temperatures of 350, 550, and 750 °C, concrete's shear capacity decreased by 18.85, 29.6, and 52.74%. As a result, concrete's shear strength may be drastically reduced if there is no transverse reinforcement across joints.

Researchers conducted studies while the structures were being heated and after they had cooled to room temperature to understand more about what happens to concrete buildings when heated to evaluate the structural element's resistance and its residual strength capacity [27]. The advancement of fire detection and firefighting equipment has significantly shortened the duration of most fire incidents. It might be difficult to determine whether a heat-damaged building can be occupied and utilized normally or needs to be renovated or completely rebuilt. Investigating what happens to concrete structures as temperature increases to room temperature is essential. Many studies on the shear strength of concrete joints have been conducted during the past 50 years. However, the majority of these investigations were carried out at room temperature. There are still a few unanswered questions regarding the shear strength. Only a few research have examined the possibility of high temperatures diminishing the shear capacity of concrete joints.

This study introduces a non-linear finite element analysis approach to investigate the shear capability of plain and RC joints after being exposed to high temperatures, where a full analysis of the results was presented from a structural point of view with a realistic and uncomplicated analytical approach being introduced for predicting the shear capacity of shear key joints under elevated temperatures. The RC model is first validated in this study using experimental data previously published by Ahmad et al. [25, 26]. Afterward, it was expanded to consider how the mechanism will be affected by the effect of high temperatures and the presence of steel stirrups. Shear-key models may be exposed to high temperatures when the structural system undergoes a fire scenario. Determining the shear capacity of the exposed concrete joint may therefore be essential. The shear strength of shear-key models heated to extremely high temperatures is examined in this work. Additionally, a straightforward approach to determining the shear capacity of heated shear-key models is proposed, and the NLFEA results were also compared with other models from the literature.

2. Nonlinear Finite Element Analysis (NLFEA)

2.1 General

Simulation using NLFEA is done by approximating the existing geometry in the real problem into the closest one in the finite element. This is also accompanied by assuming the boundary and loading conditions for simulation purposes that best describe those in the exact problem. The geometry is modeled for all the system components, with the various material being defined and assigned. However, each geometry is discretized into finite small ones using meshing. Then, the algebraic equations related to the system of finite elements are developed and solved. The structure was then developed by combining the differential equations. The models of the shear-key joint samples were generated using the ANSYS software [28]. Twenty-four full-scale shear-key models were utilized for simulation and validation

2.2 Review of experimental work

An experimental testing procedure has been carried out by Ahmad et al. [25, 26] to investigate the effect of high temperatures on the direct shear behavior of plain and RC structures using push-off specimens. As shown in Fig. 1(a), the shear plane area measured 125 mm 250 mm. The samples were loaded in a manner that caused shear stresses to develop in the shear direction. The push-off samples' vertical arms were strengthened with 12 mm bars to prevent damage from flexural loads. Since these bars do not traverse the shear plane, they do not assist in the structure's resistance to shear. Temperatures of 350, 550, and 750 °C were achieved in an electric oven and applied to the specimens. After the samples had been cooled, they were loaded in a UTM until they broke. This was done to measure the shear strength of concrete exposed to different temperatures. In order to apply the weight concentrically, the samples were maintained on a roller base that allowed for horizontal movement (Fig. 1 (b)). At a rate of 0.0167 mm/sec, test specimens were subjected to loading until they cracked. After achieving their maximal load, all of the test specimens promptly failed.



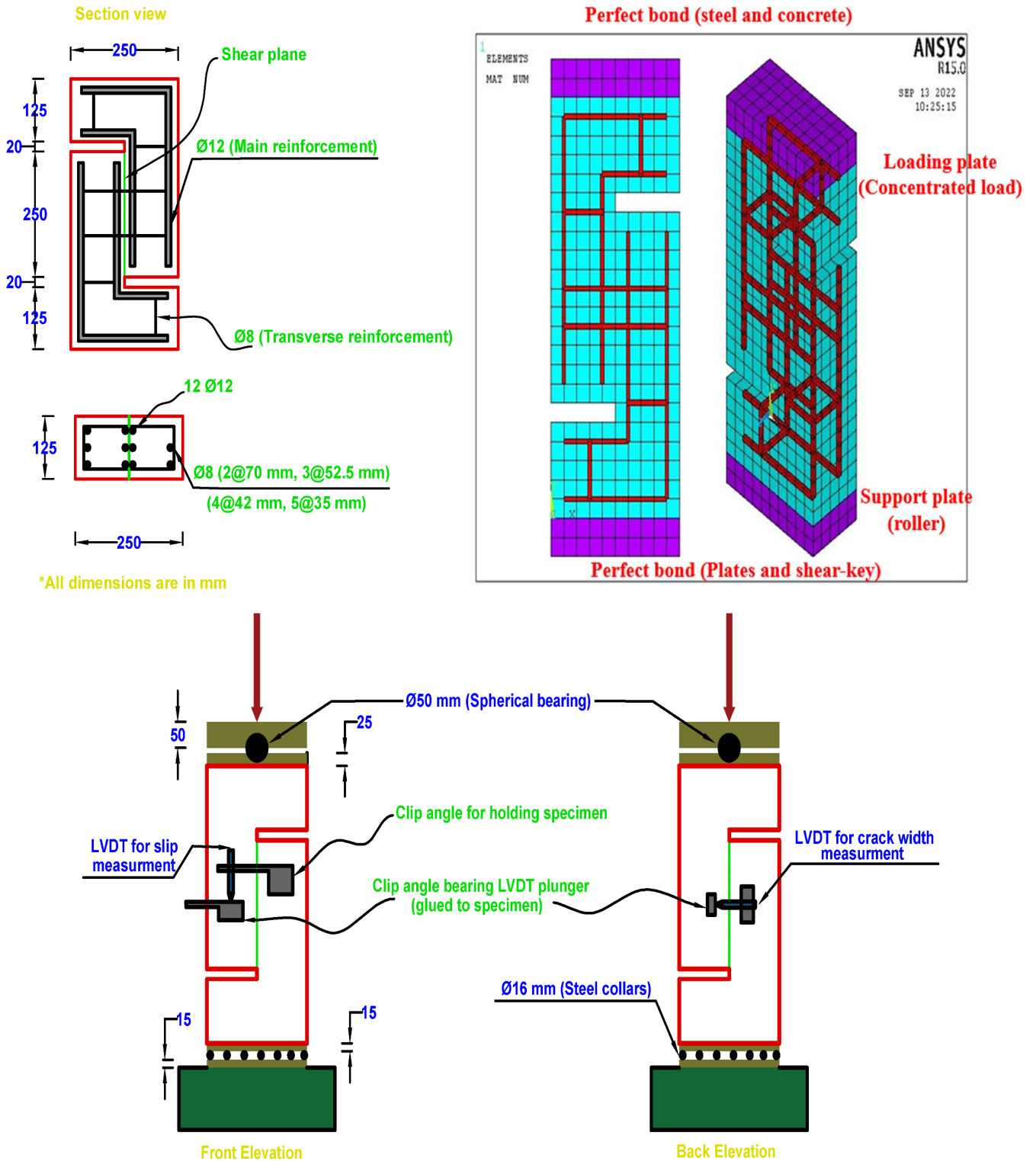


Fig. 1. Schematic diagram for the test setup, loading, and boundary conditions [25, 26].

2.3 The NLFEA's description

2.3.1 Type of element

Due to its capacity to forecast fractures in tension, crushing in compression, and plastic deformation, the SOLID65 element was utilized to describe the nonlinear behaviour of concrete. This 3D element is often used to simulate both reinforced and unreinforced solids. Each of the eight nodes that constitute the element has three degrees of freedom. There are two nodes at the borders of the steel reinforcement's discrete connection elements (LINK180), each with three degrees of freedom. Plasticity, rotation, huge strain, and deflection may all be predicted using this 3D uniaxial tension-compression spar. The steel loading plate was simulated using the SOLID185. Eight nodes define the element, each with three degrees of freedom. Homogeneous structural solids were used to represent the steel plate.



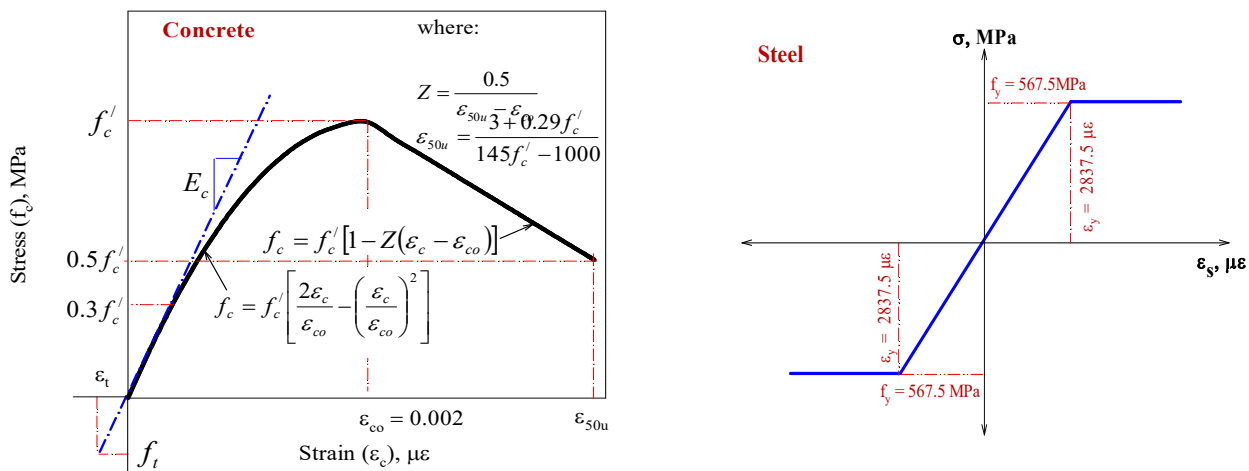


Fig. 2. Stress-strain curve for concrete and steel materials [25, 26].

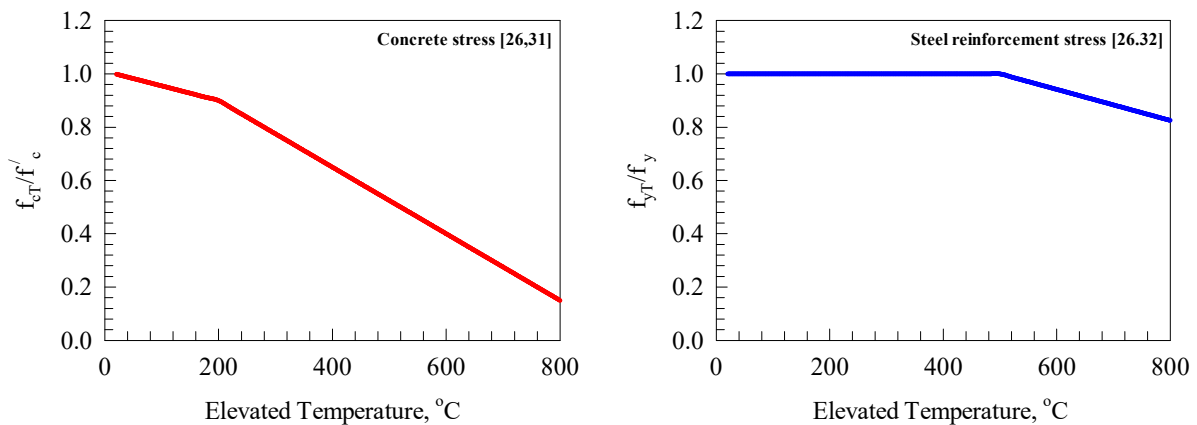


Fig. 3. Concrete and steel reinforcement stress under elevated temperatures.

2.3.2 Material characteristics

Concrete is a heterogeneous and brittle material that undergoes cracking and crushing possibilities under stress. The ultimate uniaxial tensile and compressive strengths are required to establish a failure interface for concrete, together with the other two input strength factors. The literature (Kent and Park [29]) shows that the nonlinear behaviour of concrete after fracturing and the softening behaviour following peak stress are considered. Up to roughly 30% of its compressive strength, the concrete stress-strain relationship shows a nearly linear elastic response. After this point, the concrete begins to soften gradually until it reaches its compressive strength. In addition to compressive strength, the stress-strain connection of concrete also shows strain softening before the collapse. As seen in Fig. 2(a), the softening branch of the stress-strain relationship is almost a straight line for strains larger than the equivalent strain at peak stress. ACI 318-14 [30] is used to determine the concrete tensile stress, using a linear assumption for the concrete tension softening (as seen in Fig. 2(a)). The concrete used a 30 MPa compressive strength. Bars of 12 and 8 mm in diameter were used to strengthen after being thermo-mechanically treated. A displacement controlled (UTM) was used to perform tension tests on reinforcing bars [25]. For the fine aggregate, the researchers utilized sand from a nearby river, whereas for the coarse aggregate, the researchers used gravels with a maximum nominal maximum size of 12.5 mm mined from the calcareous rock. The value for Poisson's ratio that was chosen was 0.2. This study's shear transfer coefficients for open and closed fractures were $\beta_t = 1.0$ and $\beta_c = 0.5$, respectively.

The modulus of elasticity of steel reinforcement is assumed to be 200 GPa. Poisson's ratio is assumed to be 0.30 in this bilinear isotropic model, with a yield strength of 567.5 MPa [26]. As illustrated in Fig. 2 (b) for both longitudinal and lateral reinforcing, it is anticipated to exhibit elastic-perfectly plastic behaviour similar in tension and compression. The stress was distributed more uniformly throughout the support zones by adding steel plates at the supports and loading positions. Linear elastic materials with a Poisson's ratio of 0.3 and an elastic modulus of 200 GPa were assumed for the steel plates. Figure 3(a) was posited by Chang et al. [31] and Ahmad et al. [26] to evaluate the concrete's compressive strength at different high temperatures. Figure 3 (b) was posited by Tao et al. [32] and Ahmad et al. [26] to evaluate the reinforcement's residual yield strength after being exposed to high temperatures.

2.3.3 Analysis method and failure criteria

In the event of a multiaxial stress situation, Kent and Park [29] presented failure criteria similar to the Von Mises criterion for concrete. The nonlinearity in the upward section of the 3D failure surface was disregarded as five parameters were set to form a linear-elastic stress-strain relationship. For this reason, it is possible to prevent cracking and crushing by using multi-linear isotropic plasticity in tandem with the Kent and Park model. The main failure criterion is related to the maximum principal stress, where failure occurs once the principal compressive or tensile stresses exceed those sustained by the various material components, and consequently, failure occurs [29]. Convergence of the solution induces a stress relaxation process that eliminates the principal stress orthogonal to the initial fracture direction, as shown below. It was found that the ultimate tensile strength of the concrete dropped suddenly to $T_0 \times f_t$ after the first fracture formed, then gradually decreased as a result of linear relaxation to zero. When concrete achieves compressive strength, the strength and elastic modulus are equal to zero in all directions, regardless of the load increments applied.



Table 1. Mesh sensitivity results.

Mesh Size	Number of Elements	Number of Nodes	Ultimate Load (kN)	Error %
Fine (10mm)	1543	1352	138.62	+5.9
Medium (25mm)	1054	987	130.40	-0.4
Coarse (40mm)	678	541	127.51	-3.4

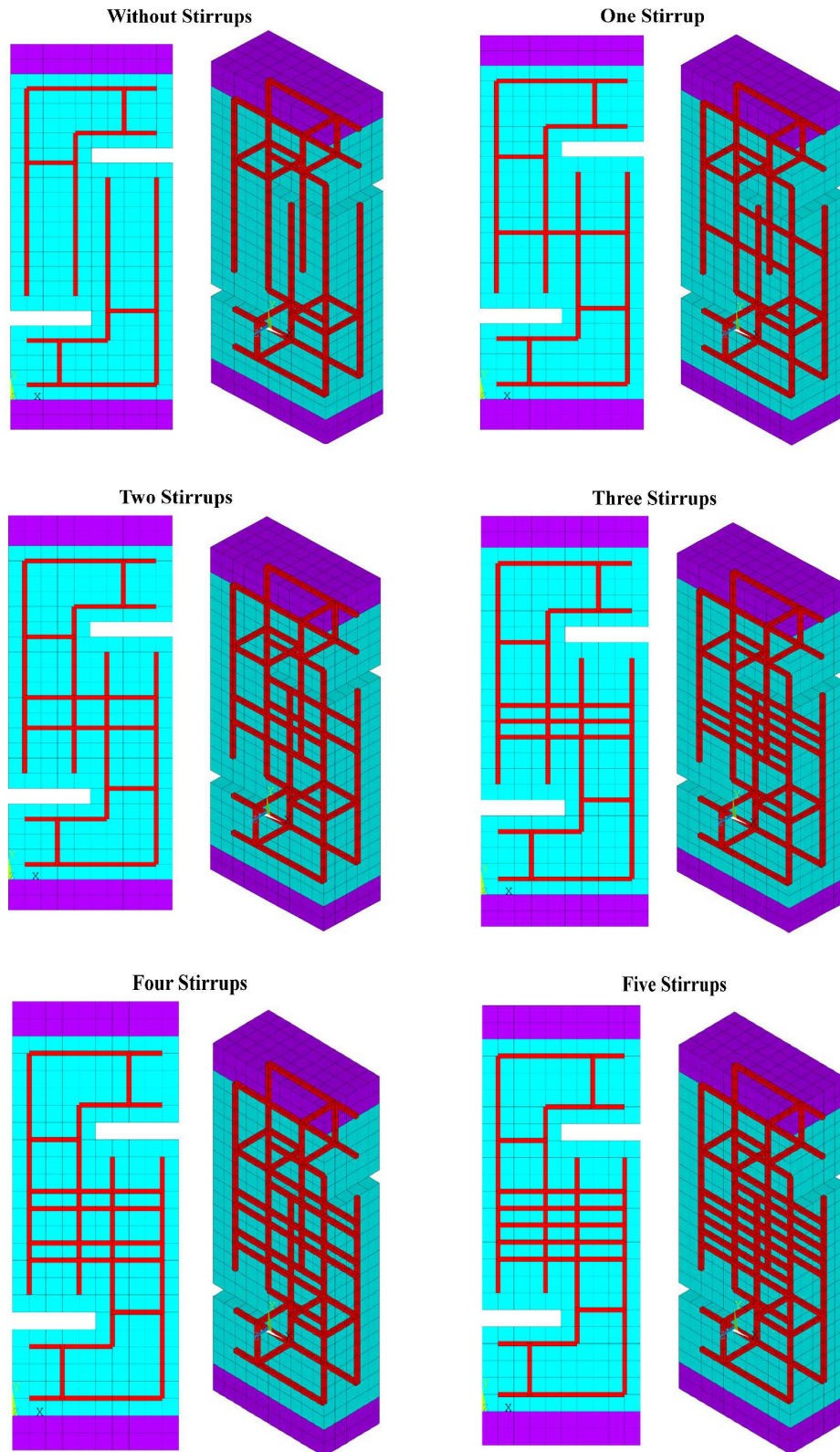


Fig. 4. Shear-key joints meshing.



Table 2. The longitudinal shear force of tested [25, 26] and NLFEA shear-key specimens.

Specimen	Ultimate load, kN			Specimen	Ultimate load, kN		
	Experimental (Average)	NLFEA	Predicted Tested		Experimental (Average)	NLFEA	Predicted Tested
(20°C) [25]	131.0	131.1	1.00	A-2 [26]	270.8	273.5	1.01
(350°C) [25]	106.3	105.3	0.99	350-2 [26]	227.7	228.8	1.01
(550°C) [25]	92.2	95.5	1.04	550-2 [26]	202.2	203.6	1.01
(750°C) [25]	61.9	59.9	0.97	750-2 [26]	151.6	152.0	1.00
A-3 [26]	303.3	288.1	0.95	A-5 [26]	379.4	352.8	0.93
350-3 [26]	266.1	274.2	1.03	350-5 [26]	327.3	320.8	0.98
550-3 [26]	225.6	241.4	1.07	550-5 [26]	284.0	272.6	0.96
750-3 [26]	166.6	181.6	1.09	750-5 [26]	209.4	222.0	1.06

The NLFEA procedure starts with modeling the geometry as various components that assemble and mesh for simplicity. The model is discretized into small finite elements where the resulted stresses, strains, and other computed values are measured at the integration points composing the local stiffness matrix that assembles all of the system components forming the global stiffness matrix that is further utilized to solve the NLFEA model. However, one of the essential steps in the finite element procedure is choosing the appropriate mesh density where the utilized mesh size highly influences the results and convergence. In this study, a mesh size of 25 mm has been used after a proper mesh sensitivity analysis was done for the ambient temperature specimen (20°C), as per Table 1 [25], considering the ultimate loading prediction and the computational time as the judging criteria. The meshed specimen is illustrated in Fig. 4. In addition, a perfect bond was assumed between the concrete and steel materials inside the simulated joints. Moreover, a perfect bond was assumed between the loading and support plates and the shear key joint. The roller boundary condition was simulated at the loading plate interface. However, the concentrated loading procedure was applied at the top of the plate. Loading was applied as substeps to ensure the solution convergence, where a 0.35 kN loading increment was applied. Furthermore, the Newton-Raphson equilibrium method with a 0.001 tolerance limit and the maximum and minimum loading steps are automated using ANSYS software [28]. Finally, the solution stops when the added force causes the solution to diverge. Furthermore, failure occurs when the maximum principal stress exceeds the material's capacity, so a solution divergent occurs.

2.4 Validation

Table 2 summarises the shear force and accompanying slip values obtained using NLFEA for the simulated shear-key samples and the equivalent experimental values (see Ahmad et al. [25,26]). There is a tiny discrepancy of about 9% between the anticipated shear force and the accompanying slide for the shear keys and the corresponding experimental data. The investigation shows that the model often accurately forecasts the shear-key behaviour of composite concrete bridges subjected to high temperatures. A total of sixteen shear-key joints have been validated, with each experimental value representing the average of two tested specimens.

2.5 Parameters investigated

The number of steel stirrups and the temperature were the only two variables used to simulate 24 push-off samples. Figure 1 and Table 3 outline the plain and RC shear-key setup and reinforcing features. Each of the six groups in the extended parametric research has four models of the same reinforcement type. High Temperatures (23 °C (Room Temperature), 250 °C, 500 °C, and 750 °C and the number of steel stirrups (0 (none), 1, 2, 3, 4, and 5) were evaluated using the researched characteristics. According to the examples provided here, the first letter indicates the higher temperatures (T23, T250, T500, and T750). The quantity of steel stirrups is as follows (S0, S1, S2, S3, S4, and S5).

3. Results and Discussion

3.1 Failure modes

The two sets of simulated shear-key models created based on the observed failure mechanism reflected the connection surface features of the plain and stirrups samples. The two main groups are illustrated in Fig. 5 and Fig. 6, representing the simple shear key joint and the shear-reinforced joint with steel stirrups, respectively. This type of failure is classified as a brittle failure since no stresses resulting from the concentric compressive load were observed in the samples during the initial stages of the investigation. As the load increased, tensions developed in the vertical arms in the push-off models. Since increased temperature causes softening of concrete and pushes the models to failure at lower loads, the effects of these stresses were mitigated in the heated models. Due to the availability of adequate flexural reinforcement, not a single specimen failed due to stresses in vertical arms. After reaching their maximum load, all the samples failed suddenly. As seen in Fig. 6, the stress distribution at the time of failure is consistent across all simulated models. Models tested at room temperature had lesser stress throughout the simulation. As seen in Fig. 5, the concrete models failed with a more uniform stress distribution as the exposure temperature was raised, suggesting that the material's brittleness decreased.

To be brittle means that a substance will break easily without first undergoing any significant deformation. Ductility may be improved by reducing brittleness. When concrete is subjected to high temperatures, the amount of deformation and energy it absorbs as elastic deformation diminishes, while the amount of energy it absorbs as plastic deformation grows irreversibly—concrete's fragility shifts as its elastic energy fraction changes relative to the overall energy fraction. Table 3 shows that heating concrete surfaces to 250 °C, 500 °C, and 750 °C decreased their shear capacity by 10%, 27%, and 57%, sequentially.

The second group's failure mode can be broken down into two distinct phases: the first phase involves brittle failure of the concrete, which is primarily localized along the bonding surface between the two blocks by the creation of the initial crack, whose opening rises with applied force until ductile failure (Fig. 7). All of the experimental samples failed in a very similar way. Neither the crack's size nor its slippage was immediately noticeable. As can be seen in Fig. 7, under loading, tiny flexural fractures appeared in the vertical limbs of the models. Since concrete softens at higher temperatures [25, 26], the flexural fractures seen in heated models were larger. Flexural failure did not occur in any samples since there was adequate flexural (main) steel. Figure 7 shows the creation of short diagonal tension at an angle to the shear plane as the load increased further. The longitudinal and transverse movement of the two parts was caused by the formation of concrete struts rotating due to the elongation of transverse strengthening between these inclined fractures. Figure 7 depicts the stress testing results on models subjected to various temperatures. Separation of concrete struts from the surface, causing spalling, was also noticed. Spalling was noticeable in the examples with more stirrups (Fig. 7).



Table 3. Various plain and RC shear-key specimen results.

Specimen	Temperature, °C	Stirrups, (φ8)	Ultimate separation, mm	Ultimate slip, mm	Ultimate load, kN	Concrete load, kN	Steel load, kN
T20S0	20	Without	0.0014	0.003	114.1	114.1	0.0
T250S0	250		0.0016	0.004	103.2	103.2	0.0
T500S0	500		0.0019	0.005	83.3	83.3	0.0
T750S0	750		0.0022	0.006	53.5	53.5	0.0
T20S1	20	1	0.0590	0.209	201.6	114.1	87.5
T250S1	250		0.0663	0.280	185.7	103.2	82.6
T500S1	500		0.0753	0.387	154.6	83.3	71.3
T750S2	750		0.0851	0.536	110.4	53.5	56.9
T20S2	20	2	0.1052	0.256	246.0	114.1	131.9
T250S2	250		0.1183	0.344	225.7	103.2	122.5
T500S2	500		0.1337	0.475	190.4	83.3	107.1
T750S2	750		0.1525	0.659	138.5	53.5	85.0
T20S3	20	3	0.1479	0.288	280.2	114.1	166.1
T250S3	250		0.1665	0.390	259.0	103.2	155.8
T500S3	500		0.1880	0.536	218.0	83.3	134.8
T750S3	750		0.2132	0.744	161.6	53.5	108.1
T20S4	20	4	0.1891	0.313	310.4	114.1	196.3
T250S4	250		0.2117	0.422	286.3	103.2	183.1
T500S4	500		0.2397	0.586	242.9	83.3	159.6
T750S4	750		0.2725	0.809	181.2	53.5	127.7
T20S5	20	5	0.2275	0.335	337.5	114.1	223.4
T250S5	250		0.2561	0.453	311.5	103.2	208.3
T500S5	500		0.2893	0.624	265.2	83.3	181.9
T750S5	750		0.3279	0.867	203.2	53.5	144.5

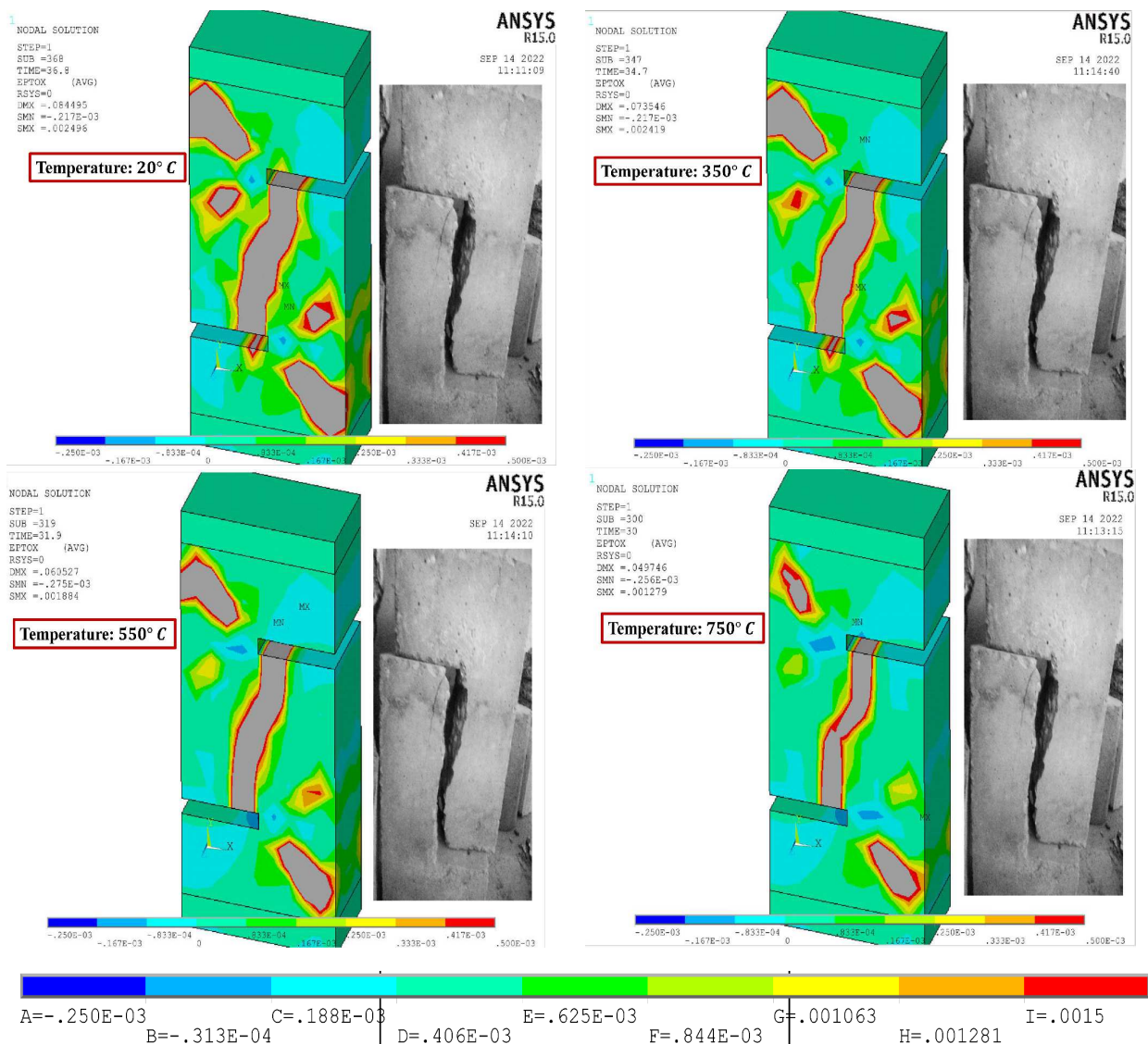


Fig. 5. Failure modes of group one (without stirrups) [25].



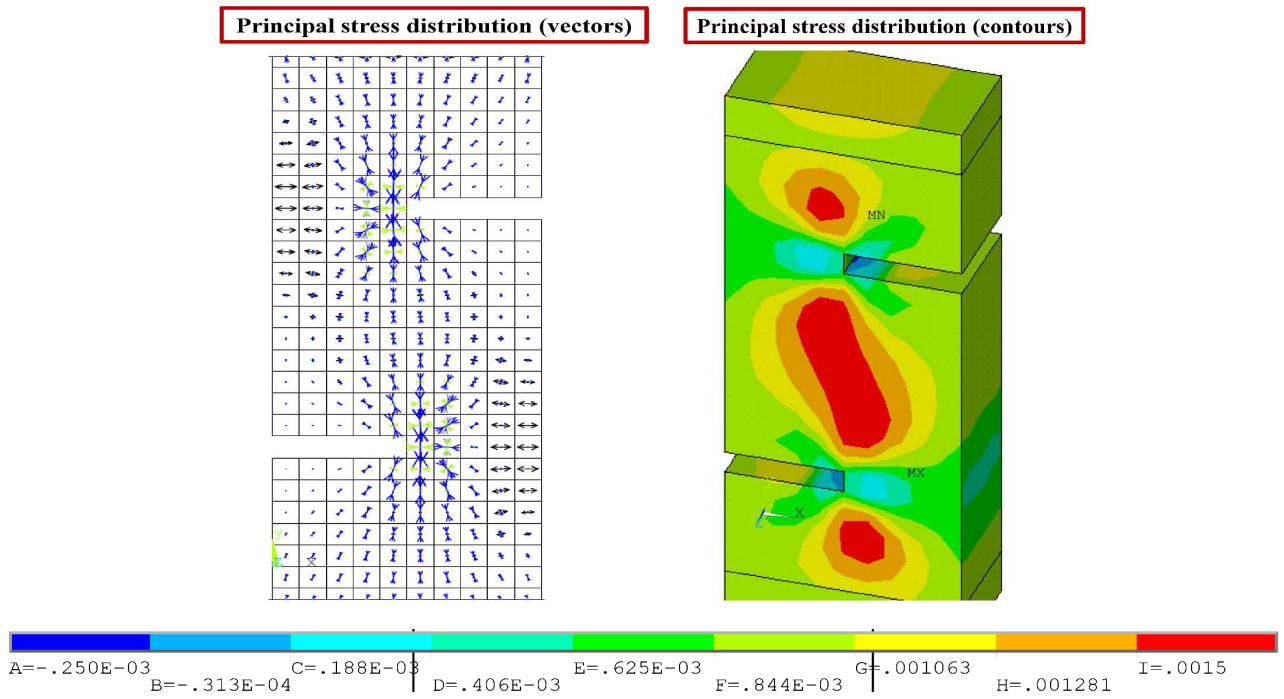


Fig. 6. Principal stress distribution in the shear-key models.

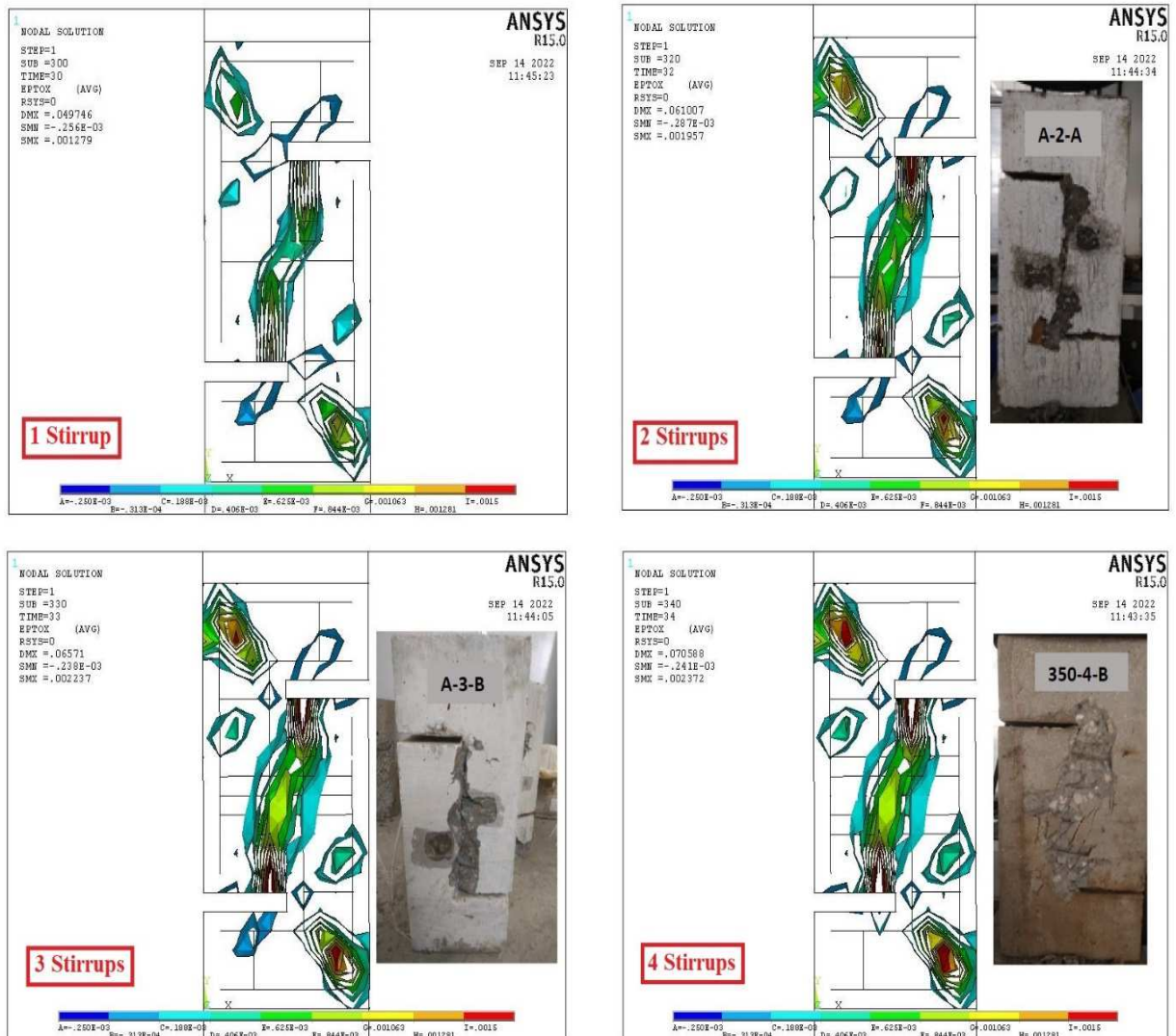


Fig. 7. Failure modes of group two (with stirrups) [26].



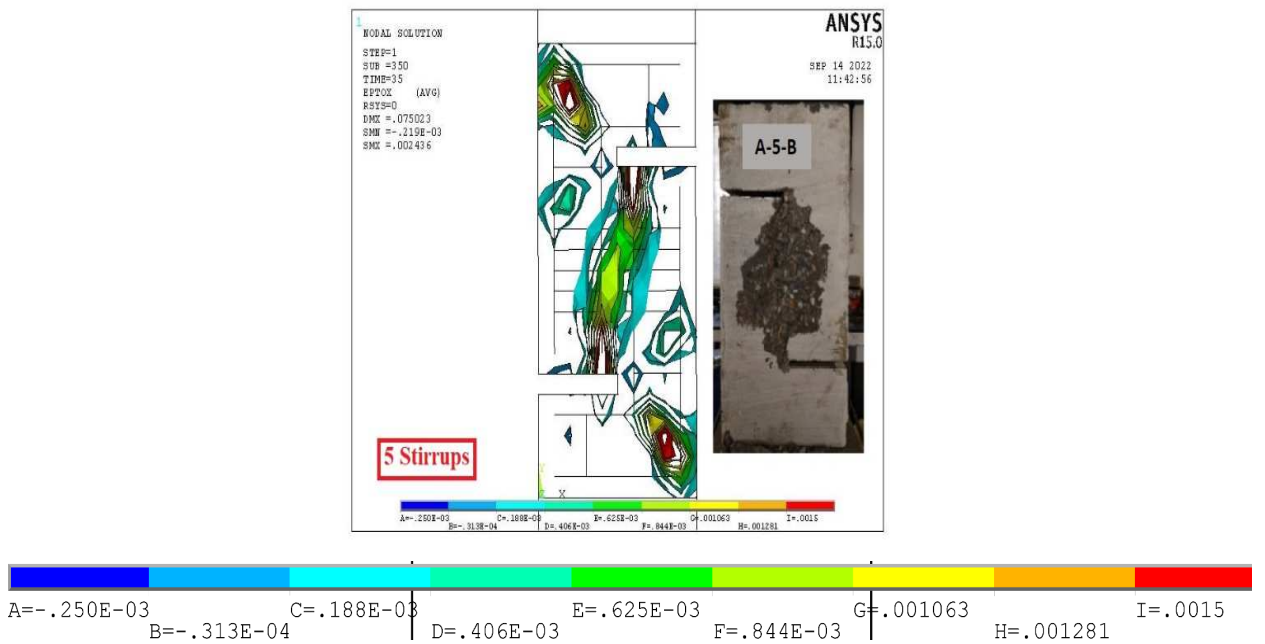


Fig. 7. Continued.

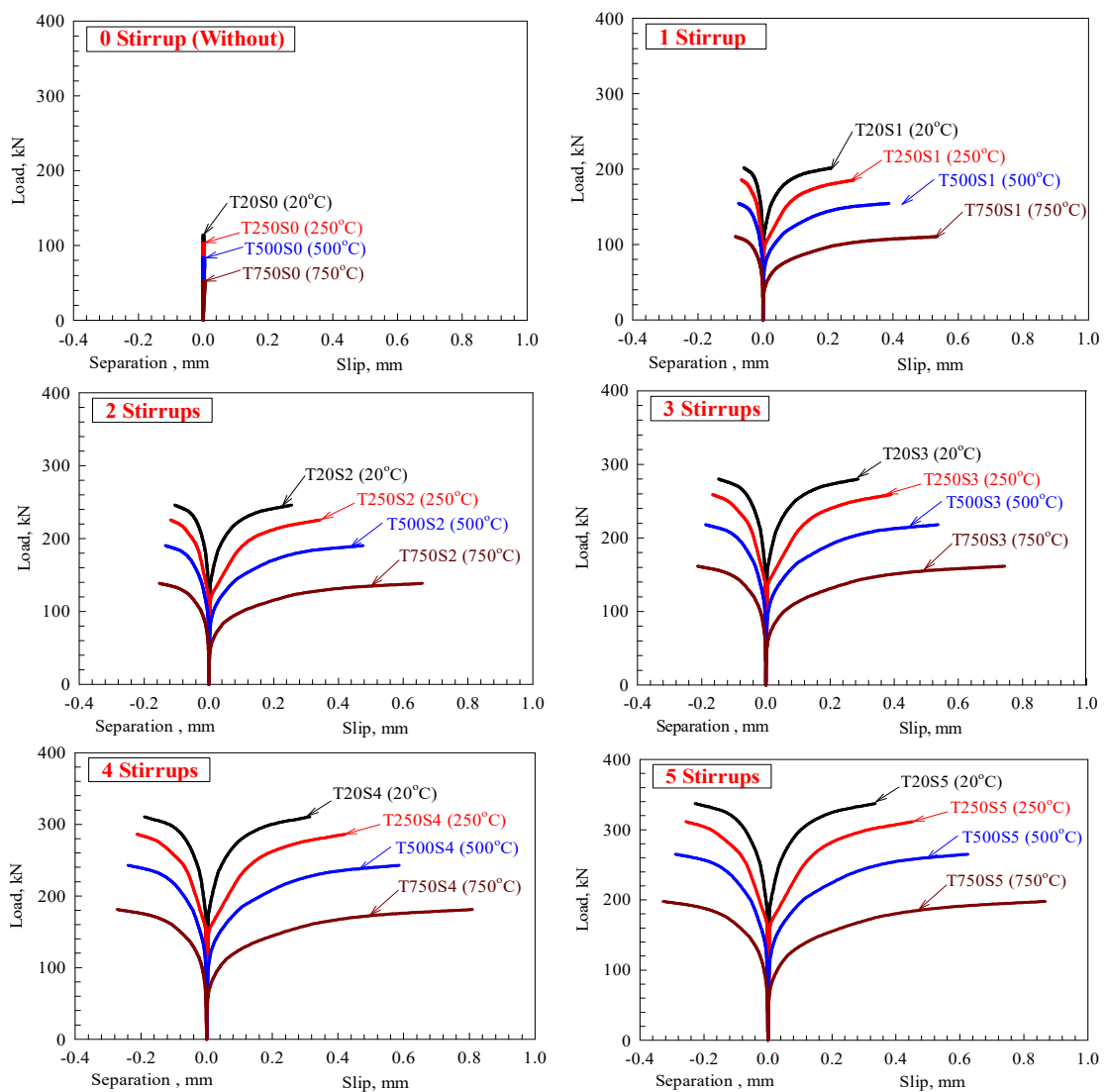


Fig. 8. NLFEA load versus slip and separation curves.



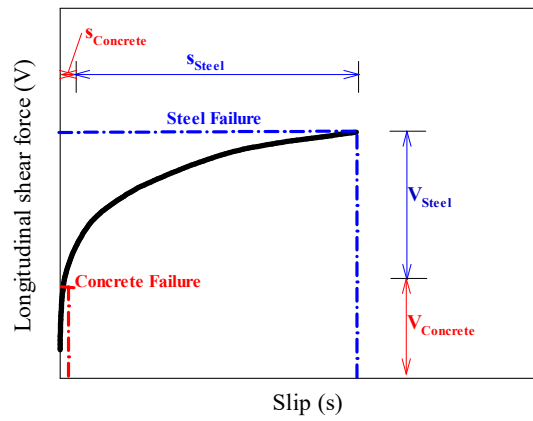


Fig. 9. Load versus slip stages.

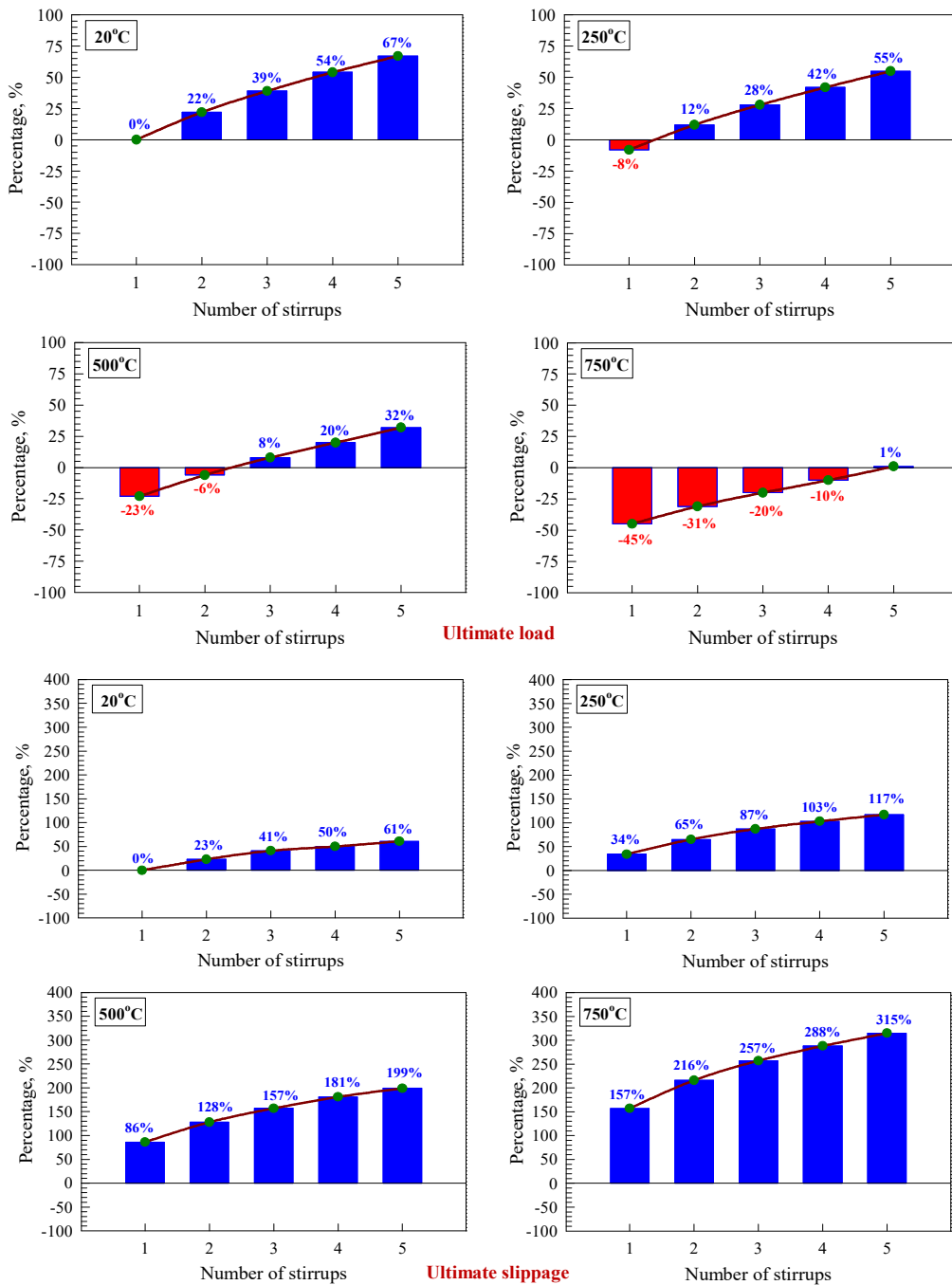


Fig. 10. Percentages of ultimate load and ultimate slippage percentages versus number of stirrups.



Table 4. Stiffness, toughness, and performance factors of NLFEA shear-key models.

Specimen	Temperature, °C	Stirrups, (ϕ8)	Stiffness, kN/mm	Toughness, kN.mm	Strength factor	Ductility factor	Performance factor
T20S1	20	1	16952	37	1.000	1.000	1.000
T250S1	250		2236	45	0.921	1.343	1.237
T500S1	500		1172	52	0.767	1.857	1.424
T750S2	750		735	51	0.547	2.570	1.407
T20S2	20		17020	56	1.220	1.228	1.498
T250S2	250	2	2236	67	1.119	1.648	1.844
T500S2	500		1188	78	0.944	2.280	2.152
T750S2	750		757	78	0.687	3.160	2.171
T20S3	20		17253	72	1.389	1.379	1.916
T250S3	250		2262	87	1.285	1.869	2.401
T500S3	500	3	1206	101	1.081	2.572	2.781
T750S3	750		783	103	0.801	3.569	2.860
T20S4	20		17543	86	1.539	1.503	2.313
T250S4	250		2308	104	1.420	2.025	2.876
T500S4	500		1229	123	1.205	2.811	3.386
T750S4	750	4	807	126	0.899	3.880	3.486
T20S5	20		17844	100	1.674	1.606	2.688
T250S5	250		2342	121	1.545	2.172	3.355
T500S5	500		1260	143	1.315	2.994	3.938
T750S5	750		824	147	0.982	4.155	4.080

Note: Performance factor = Strength factor × Ductility factor

3.2 Load slippage behavior

Fig. 8 shows the shear force against slippage and shear force against separation response curves for many shear-key models. In addition, it shows that the shear load and slip for the stirrup-equipped shear-key models were greater than those for the plain shear-key specimen. A higher number of steel stirrups also resulted in a higher shear force and more slippage. Figure 9 depicts how the NLFEA findings and failure mechanism may categorize the longitudinal shear force versus slip behaviour into two distinct phases. In the first phase, concrete contributes nearly as much as steel stirrups, which is between 31% (5 stirrups) and 54% (1 stirrup) of the ultimate longitudinal shear force. In the second phase, steel stirrups contribute nearly as much as concrete, between 69% (5 stirrups) and 46% (1 stirrup).

Moreover, as shown in Fig. 8, the fractured slide and crack separation started at smaller shear forces when models were subjected to increased temperatures. As the temperature increases, the shear stress at which the shear plane begins its longitudinal or transverse movement decreases. This finding shows that the initial stiffness of the shear plane reduces with increasing exposure Temperature. Table 4 and Fig. 8 show that the shear strength decreases when the exposure temperature rises and the shear plane deforms more at each stress level. After being subjected to high temperatures, the models underwent lower and ductile shear transfers. It was shown that concrete cohesiveness, aggregate interlock, and transverse reinforcement given across a shear plane all contribute to the successful transmission of shear forces [25, 26].

Compared to a specimen reinforced with a single steel stirrup at 20 °C, Fig. 10 displays the percentage increase or decrease in ultimate load and accompanying slippage as a function of the number of stirrups used in the reinforcement. The ultimate load capacity of the shear-key models was increased by 22%, 39%, 54%, and 67% sequentially when subjected to 20 °C (Room Temperature) and strengthened with 2, 3, 4, and 5 steel stirrups, sequentially (Fig. 10(a)). For 2, 3, 4, and 5 steel stirrups, the corresponding increases in ultimate slippage were 23%, 41%, 50%, and 61%, respectively (Fig. 10(b)). The high temperature of 250 °C had a moderate effect, decreasing the ultimate load by 8% for samples strengthened with one stirrup and increasing the ultimate load of remainder models with an increase of steel stirrups by an average of 29% with regard to 20 °C.

For samples strengthened with one stirrup, the ultimate load decreased by 23%, while for samples strengthened with two stirrups, the ultimate load decreased by 6% due to the higher temperature of 500 °C. The average decrease percentage was only 63.5% with regard to 20 °C, and the final weight of the rest models rose with the number of steel stirrups. For samples strengthened with 1, 2, 3, and 4 stirrups, sequentially, the ultimate load decreased by 45%, 31%, 20%, and 10% when subjected to an enhanced Temperature of 750 °C. At 20 °C, a 1% increase in enhancement leads to a 1.5% increase in ultimate load when using five stirrups. This explains why it is needed at least 1, 2, or 5 steel stirrups, depending on the temperature, to restore the strength lost at 250 °C, 500 °C, or 750 °C, sequentially.

3.3 Toughness

Due to girder-slab relative slip, longitudinal shear force deformations are expected (two blocks). Toughness is connected to effectiveness and dynamic loadings throughout Table 4, making it a key element of composite bridges—the area beneath the load-slip curve measures shear-keys' energy-absorption capability. At 20 °C, Fig. 11 displays the proportion of increase or decrease in toughness in relation to the number of steel stirrups used to support the models, with 2, 3, 4, and 5 steel stirrups showing increases in the toughness of 50%, 97%, 131%, and 169% at room temperature (20 °C) (Fig. 11). As the temperature was raised, the ultimate slippage grew rapidly. In contrast, the ultimate shear force decreased slowly, resulting in a proportional rise in the toughness enhancement percentages. As a result, the steel stirrups slowed the progression of the diagonal cracks by bridging and carrying loads over the contact region, which increased the final slippage and delayed the beginning of the first shear cracking. This improved the ultimate shear cracking load and toughness of shear-key models of strengthened concrete under service load circumstances.

3.4 Separation

Whenever a load is added, the separation or crack opens. As the applied load was increased after the crack's formation, separation and slide also increased, eventually leading to collapse. When comparing the shear force against slip response to the separation against slip response, it is found that they are mirror images of one another (Fig. 8). Roughness of the RC shear keys plane surface may be inferred from its separation or crack opening against slip response. For shear keys equipped with stirrups, however, the separation against slip response indirectly indicates the effectiveness of the total number of stirrups. Steeper separation against slide behaviour in shear-keys often absorbs more energy before fractures. Figure 8 shows that the steel stirrups increased strength and lowered separation values for the same load.



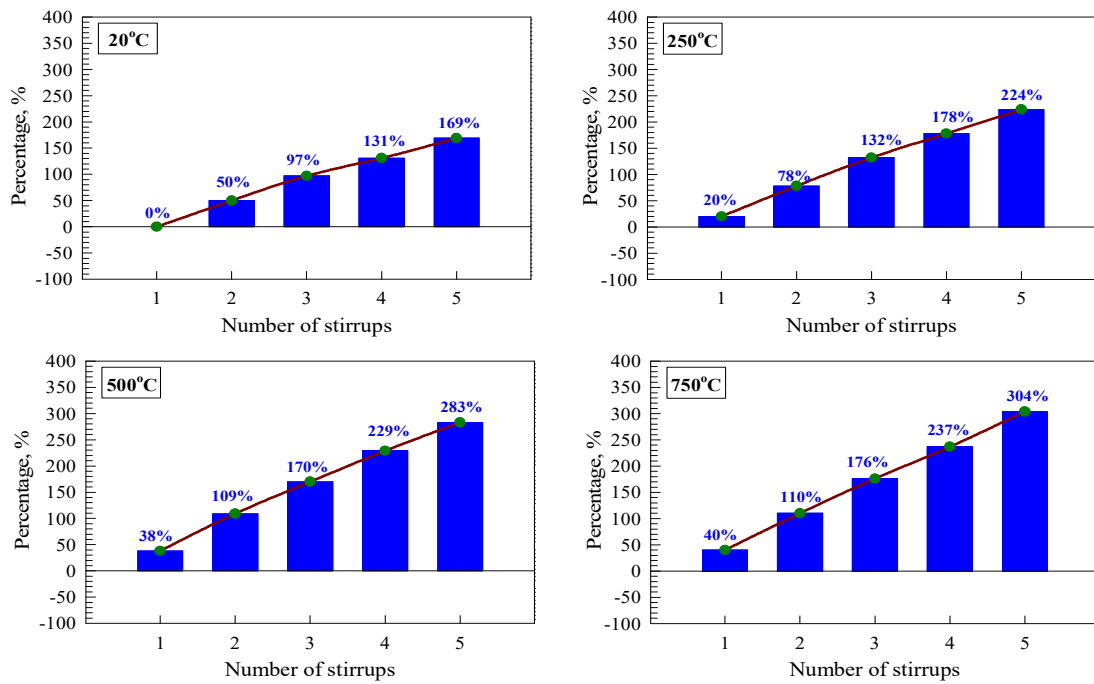


Fig. 11. Toughness percentages versus number of stirrups.

3.5 Evaluation of performance

In this scenario, the ultimate load capacity and the related slippage of the RC shear key may be used to establish the ultimate load limit and serviceability states. Using the safe and sound control RC shear key strengthened with one stirrup at room temperature as a benchmark, calculating the deformability factor (DF) and the strength factor (SF) of the RC shear-key models is possible. A performance factor (PF), defined as DF multiplied by SF, may be used to assess the overall structural performance of shear-key models. Therefore, the SF, DF, and PF for various RC shear-key models are used to assess the performance of shear key-joints, as shown in Table 4. The values of the performance, strength, and deformability factors all rose as the number of stirrups grew, as shown in Table 4. Saving the original strength of the control RC specimen is impossible, as shown by the SF being less than one. Furthermore, at temperatures of 250 °C, 500 °C, and 750 °C, the bare minimum of steel stirrups to utilize is sequentially 2, 3, and 5.

4. Interface Shear Strength Capacity Prediction

Different models have been proposed in the literature for predicting concrete behavior under ambient temperature conditions. Mattock [33] has figured out a model to predict the shear strength of reinforced concrete joints, as shown in Eq. (1). Regression was used to assess the results of an experimental investigation carried out at the University of Washington, and this method of backward verification was used to construct the model:

$$V_u = 0.467(f_c')^{0.545} A_c + 0.8A_v f_y \tag{1}$$

where V_u is the ultimate longitudinal shear strength of RC joint, f_c' is the concrete 28-day compressive strength, steel stirrups have yield strength of f_y at room temperature, where A_c is the area of the shear plane, A_v is the area of the stirrups inside the shear plane. Kahn and Mitchell [16] tested fifty push-off samples to estimate reinforced concrete interface shear capacity:

$$V_u = 0.05f_c' A_c + 1.4A_v f_y \tag{2}$$

The following equation can determine the shear strength of surfaces exposed to high temperatures, as presented by Ahmad et al. [25, 26]:

$$V_u = 0.6\sqrt{f_{cT}} A_c + \mu_T A_v f_{yT} \tag{3}$$

For a given temperature T , the concrete's compressive strength and the yielding stress of steel reinforcement are sequentially denoted by f_{cT} and f_{yT} . Both f_{cT} and f_{yT} may be calculated using equations (6) and (7) from Chang et al. [31] and Tao et al. [32]. Concrete's coefficient of friction at a high-temperature T is denoted as μ_T . In order to calculate μ_T , equation (8) from Ahmad et al. [26] can be used:

$$f_{cT} = \begin{cases} (1.01 - 0.00055T)f_c' & 20^\circ C \leq T \leq 200^\circ C \\ (1.15 - 0.00125T)f_c' & 200^\circ C \leq T \leq 800^\circ C \end{cases} \tag{4}$$

$$f_{yT} = \begin{cases} f_y & T \leq 500^\circ C \\ (1 - 0.0000582(T - 500))f_y & 500^\circ C \leq T \end{cases} \tag{5}$$

$$\mu_T = -0.000006T^2 + 0.0001T + 0.8259 \quad 20^\circ C \leq T \leq 750^\circ C \tag{6}$$



Table 5. NLFEA and predicted shear capacities of shear-key models.

Specimen	T, °C	V _{NLFEA} , kN	Mattock [33]		Kahn and Mitchell [16]		Ahmad et al. [25, 26]		Proposed Model (Eq. 9)	
			V _u , kN	V _u /V _{NLFEA}	V _u , kN	V _u /V _{NLFEA}	V _u , kN	V _u /V _{NLFEA}	V _u , kN	V _u /V _{NLFEA}
T20S1	20	114.1	121.1	1.061	60.9	0.534	102.6	0.900	113.5	0.995
T250S1	250	103.2	101.0	0.979	51.0	0.495	94.0	0.911	103.2	1.000
T500S1	500	83.3	79.7	0.957	32.0	0.384	74.4	0.894	83.0	0.997
T750S2	750	53.5	49.6	0.927	12.9	0.242	47.3	0.885	53.5	1.001
T20S2	20	201.6	152.6	0.757	112.8	0.559	154.6	0.767	201.7	1.000
T250S2	250	185.7	132.5	0.713	102.9	0.554	145.0	0.781	185.2	0.997
T500S2	500	154.6	111.2	0.719	83.9	0.543	119.9	0.776	154.4	0.999
T750S2	750	110.4	76.5	0.693	57.3	0.519	77.5	0.702	110.4	1.000
T20S3	20	246.0	184.1	0.748	164.7	0.669	206.5	0.839	245.3	0.997
T250S3	250	225.7	164.0	0.727	154.8	0.686	196.0	0.869	225.7	1.000
T500S3	500	190.4	142.7	0.750	135.8	0.713	165.5	0.869	189.8	0.997
T750S3	750	138.5	103.4	0.747	101.6	0.734	107.7	0.778	138.6	1.001
T20S4	20	280.2	215.6	0.770	216.5	0.773	258.4	0.922	280.2	1.000
T250S4	250	259.0	195.5	0.755	206.7	0.798	247.0	0.954	258.2	0.997
T500S4	500	218.0	174.2	0.799	187.7	0.861	211.0	0.968	218.1	1.000
T750S4	750	161.6	130.3	0.807	146.0	0.903	137.9	0.854	161.1	0.997
T20S5	20	310.4	247.1	0.796	268.4	0.865	310.3	1.000	310.5	1.000
T250S5	250	286.3	227.0	0.793	258.6	0.903	298.1	1.041	286.4	1.000
T500S5	500	242.9	205.7	0.847	239.6	0.986	256.5	1.056	242.6	0.999
T750S5	750	181.2	157.3	0.868	190.3	1.050	168.1	0.928	180.6	0.997

Note: V_{NLFEA} is the NLFEA shear capacities and V_u is the predicted shear capacities

4.1 Prediction of concrete interface shear capacity

Concrete compressive strength is the most significant characteristic that describes concrete behavior since it is well-known as strong material in compression and weak in tension. Moreover, other sensitive parameters affect the overall behavior, including the normal stress distribution along the joint interface and its type, the steel reinforcement ratio, the bars diameter, and the percentage of steel provided within the interface.

In the literature, various models for calculating the shear strength of a concrete interface have been developed, each based on a unique collection of data from experimental and mathematical research [16, 33, 25, 26]. The following structure describes the vast majority of these models:

$$V_u = C A_c + \mu A_v f_y \quad (7)$$

$C_T A_c$ and $\mu_T A_v f_y$ represent the shear resistance provided by concrete and steel. The coefficient of friction on the surface of the fracture. The steel's contribution is the combined resistance of the shear strengthening placed across the interface and the frictional shear placed at the fracture's surface. Equations (2) to (5) verify that the model developed by Ahmad et al. [25, 26] correctly predicted the increased shear capacity of the RC shear-key models subjected to increasing temperatures. The same concept is used to figure out how much shear capacity shear-key models of strengthened concrete have when heated up. From equation (7), it is noted that the total shear capacity of a strengthened concrete joint is the sum of the concrete contribution and the steel contribution. The following equation can be used to determine how strong a connection between two pieces of strengthened concrete is when heated to a high temperature:

$$V_u = C_T A_c + \mu_T A_v f_y \quad (8)$$

The concrete and steel reinforcement contribution within the longitudinal shear force capacity of the shear key joints are represented by C and T , respectively, as shown in Fig. 12. The following are some general formulations for determining the maximum longitudinal shear force, which may be obtained by substituting the values of these coefficients (Fig. 12) into equation (8):

$$V_u = \left(-0.00000043524T^2 \sqrt{f'_c} - 0.00014508T \sqrt{f'_c} + 0.6664008 \sqrt{f'_c} \right) A_c + \left(-0.00000056T^2 n_s^{0.58} - 0.00032T n_s^{0.58} + 1.55248 n_s^{0.58} \right) A_v f_y \quad (9)$$

4.2 Literature models

Table 5 and Fig. 13 summarise the NLFEA to expected shear capacity (V_{NLFEA}/V_u) ratios from the models of Mattock [33], Kahn and Mitchell [16] as well as Ahmad et al. [25, 26]. The mean V_{NLFEA}/V_u calculated using Mattock's [30] model was 0.820, with a coefficient of variation of 11.3%. Consequently, the equation of Mattock [33] may be used to reliably determine the shear strength of interfaces. Kahn and Mitchell's model [16] predicts a shear capacity for NLFEAs that is 0.749% lower than observed values. According to the concept of Kahn and Mitchell [16], the shear resistance of concrete should only amount to 5% of its strength. This means that the test data is best explained by a coefficient of friction that is 1.4 times greater than typical. Furthermore, the approach of Kahn and Mitchell [16] is not suitable for estimating the shear strength of the plain concrete surface because the contribution is given exclusively to uncracked concrete. The most precise approach is that Ahmad et al. [25, 26] proposed, which resulted in a mean V_{NLFEA}/V_u of 0.917 with a variation coefficient of 12.3%. In addition, it is important to note that the predictions for the samples subjected to testing at surrounding and 250 °C were appropriate and cautious, which became too conservative at 500 °C and 750 °C. Internal cracking and brittleness occur when concrete is repeatedly heated and cooled [25, 26]. The ratio V_{NLFEA}/V_u rises because when the exposure temperature rises, the number of cracks in the concrete also rises.



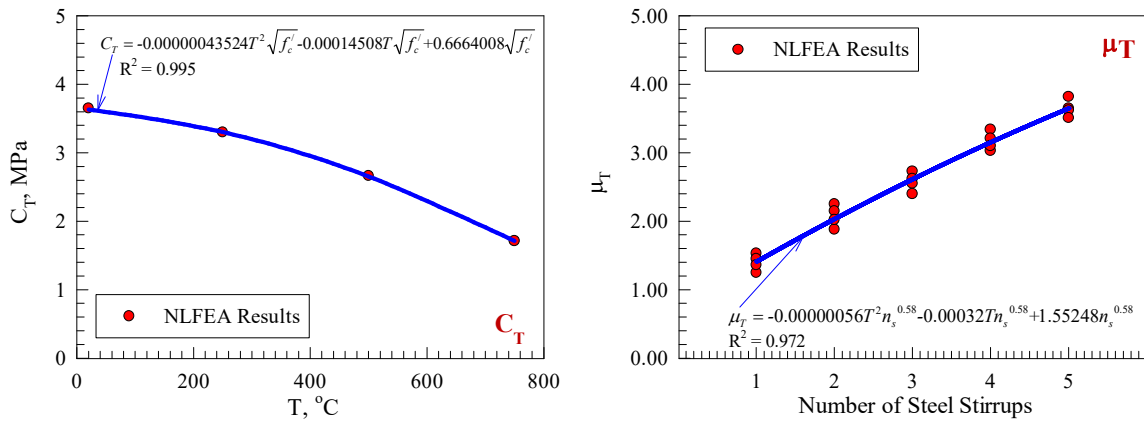


Fig. 12. Regression analysis coefficients.

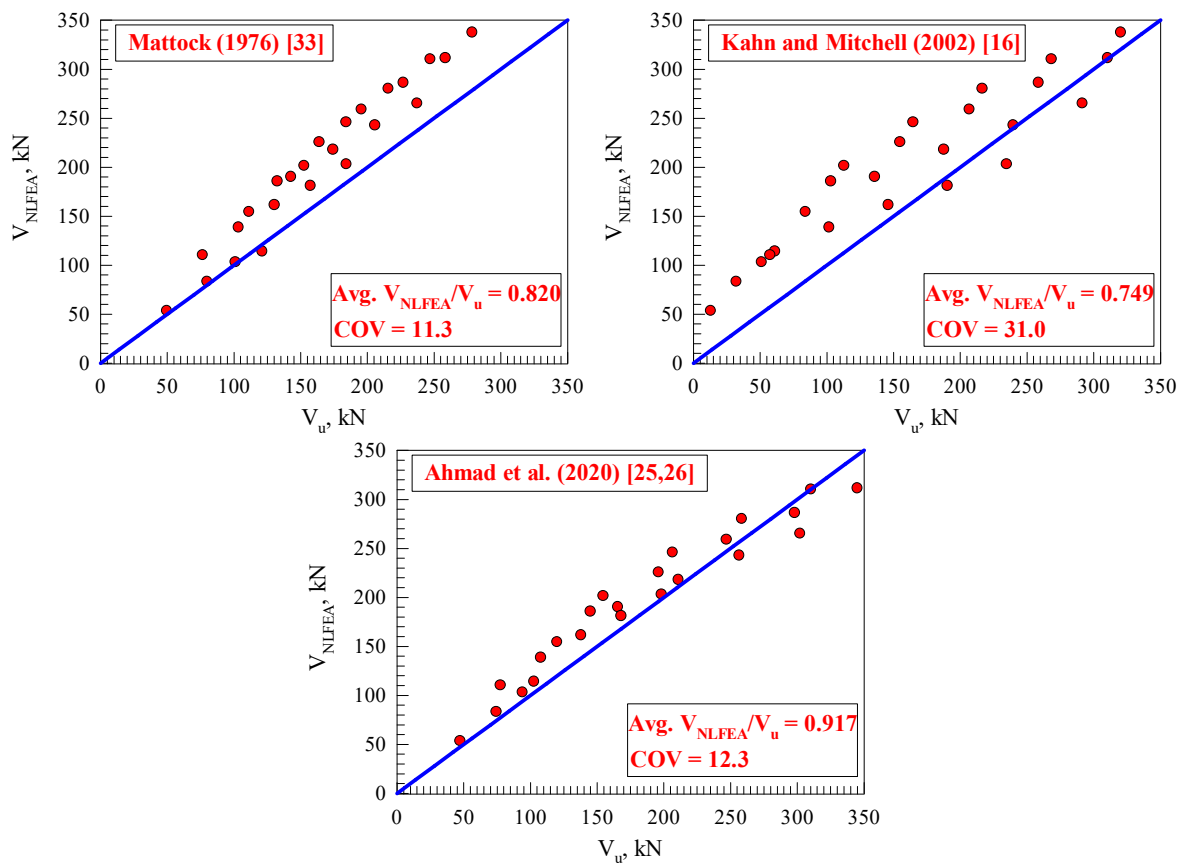


Fig. 13. NLFEA and predicted shear capacities of shear-key models

5. Conclusions

This NLFEA inquiry aimed to determine the effect of elevated temperatures on the shear capacity of plain concrete and RC shear-key models. For the assessment of the shear capacity of NLFEA models, the behaviour of several models after including the concrete’s residual strength was also investigated. The key findings are as follows:

1. Exposure Temperatures of 250 °C, 500 °C, and 750 °C resulted in average percentage decreases of 8%, 23%, and 45%, sequentially, in the shear capacity of the concrete shear-key models.
2. The steel stirrups significantly affected the longitudinal shear force, slide, failure mode, and toughness.
3. The shear capacity of concrete material is significantly reduced under increasing the exposed temperature, and this reduction is proportional to the square root value of the compressive strength, as stated in equation (9).
4. With plain concrete shear keys, the load-slip and separation-slip responses are direct indicators of reducing the roughness of the shear plane surface with increasing exposure to increased temperatures, but for RC shear keys, they may be interpreted as an indirect indicator of the effectiveness of the steel stirrup count.
5. The shear capacities of plain concrete shear-key models were reasonably and conservatively estimated using the model of Mattock [30] that included high-temperature concrete strength, whereas the shear capacities of RC shear-key models were underestimated.
6. In all temperature ranges, the shear capacities of the shear-key models were estimated conservatively using the method suggested by Kahn and Mitchell [16].



7. The shear capacity of the NLFEA shear-key models was accurately predicted after using the increased temperature concrete strength in the model of Ahmad et al. [25, 26]. The shear capacity of plain and RC shear-key models subjected to increased temperatures is thus recommended to be evaluated using the model of Ahmad et al. [25, 26] that incorporates residual concrete strength.
8. Regarding heat-damaged shear-key models, a new model is suggested to estimate the damage level in the ultimate, which may assist engineers in designing an optimal amount of steel stirrups.

Author Contributions

R.Z. Al-Rousan planned the scheme, initiated the project, suggested the experiments, conducted the experiments and analyzed the empirical results, developed the mathematical modeling and examined the theory validation. The manuscript was written through the contribution of all authors. All authors discussed the results, reviewed, and approved the final version of the manuscript.

Acknowledgments

The authors gratefully acknowledge the technical support from the Deanship of Scientific Research at Jordan University of Science and Technology.

Conflict of Interest

The authors declared no potential conflicts of interest concerning the research, authorship, and publication of this article.

Funding

The authors received no financial support for the research, authorship, and publication of this article.

Data Availability Statements

The datasets generated and/or analyzed during the current study are available from the corresponding author on reasonable request.

Nomenclature

NLFEA	Nonlinear finite element analysis	A_c	The area of the shear plane
β_t	Shear transfer coefficients for open fracture	A_v	The area of the stirrups
β_c	Shear transfer coefficients for closed fracture	$f_c T$	The concrete 28-day compressive strength at specific temperature
DF	Deformability factor	$f_y T$	Yield strength of steel at specific temperature
SF	Strength factor	CA_c	Shear resistance provided by concrete
PF	Performance factor	$\mu A_v f_y$	Shear resistance provided by steel
V_u	The experimental ultimate longitudinal shear strength of RC joint	V_{NLFEA}	The NLFEA ultimate longitudinal shear strength of RC joint
f'_c	The concrete 28-day compressive strength	CV	Coefficient of variation
f_y	Yield strength of steel	UTM	Universal Testing Machine
RC	Reinforced Concrete	3D	Three-dimensional
ACI	American Concrete Institute	f_t	Concrete tensile strength
T_0	Initial exposure temperature	C_T	Concrete shear factor
n_s	Number of steel stirrups	T	Temperature
μ_T	Steel shear factor		

References

- [1] Ye, M., Li, L., Li, H., Zhou, C., Shear behavior of joints in precast UHPC segmental bridges under direct shear loading, *Construction and Building Materials*, 357, 2022, 129212.
- [2] Liu, T., Wang, Z., Long, Z., Zeng, J., Wang, J., Zhang, J., Direct Shear Strength Prediction for Precast Concrete Joints Using the Machine Learning Method, *Journal of Bridge Engineering*, 27(5), 2022, 04022026.
- [3] Ahmed, G.H., Aziz, O.Q., Shear strength of joints in precast posttensioned segmental bridges during 1959–2019, review and analysis, *Structures*, 20, 2019, 527–542.
- [4] Santos, P.M.D., Júlio, E.N.B.S., A state-of-the-art review on shear-friction, *Engineering Structures*, 45, 2012, 435–448.
- [5] Jiang, H., Feng, J., Liu, A., Liang, W., Tan, Y., Liang, H., Effect of specimen thickness and coarse aggregate size on shear strength of single-keyed dry joints in precast concrete segmental bridges, *Structural Concrete*, 20(3), 2019, 955–970.
- [6] Pan, R., Cheng, L., He, W., Zhou, X., Shen, X., Direct shear performance of UHPC Multi-Keyed epoxy joint, *Structures*, 44, 2022, 1898–1909.
- [7] Ahmed, G.H., Aziz, O.Q., Shear behavior of dry and epoxied joints in precast concrete segmental box girder bridges under direct shear loading, *Engineering Structures*, 182, 2019, 89–100.
- [8] Ye, M., Li, L., Yoo, D.-Y., Li, H., Shao, X., Zhou, C., Mechanistic understanding of precast UHPC segmental beams with external tendons and epoxy joints subject to combined bending and shear, *Engineering Structures*, 280, 2023, 115698.
- [9] Al-Rousan, R.Z., Qudaisat, M.S., Single keyed joints behaviour and capacity formulation under direct shear using non-linear finite-element analysis, *Structures*, 47, 2023, 911–924.
- [10] Hu, M., Jia, Z., Han, Q., Ni, Y., Jiao, C., Long, P., Shear behavior of innovative high performance joints for precast concrete deck panels, *Engineering Structures*, 261, 2022, 114307.
- [11] Al-Rousan, R.Z., Alnemrawi, B.R., Punching shear code provisions examination against the creation of an opening in existed RC flat slab of various sizes and locations, *Structures*, 49, 2023, 875–888.
- [12] Liu, T., Wang, Z., Guo, J., Wang, J., Shear Strength of Dry Joints in Precast UHPC Segmental Bridges: Experimental and Theoretical Research, *Journal of Bridge Engineering*, 24(1), 2019, 04018100.
- [13] Zhan, Y., Li, Z., Chen, Z., Shao, J., Yue, F., John Ma, Z., Zhao, S., Experimental and numerical investigations on shear behavior of large keyed tooth joints, *Construction and Building Materials*, 344, 2022, 128200.



- [14] Kucharski, D.M., Pinto, V.T., Rocha, L.A., dos Santos, E.D., Fragassa, C., Isoldi, L.A., GEOMETRIC ANALYSIS BY CONSTRUCTAL DESIGN OF STIFFENED STEEL PLATES UNDER BENDING WITH TRANSVERSE I-SHAPED OR T-SHAPED STIFFENERS, *Facta Universitatis-Series: Mechanical Engineering*, 20(3), 2022, 617-632.
- [15] Balokhonov, R., Romanova, V., Zemlianov, A., A mesoscopic analysis of a localized shear band propagation effect on the deformation and fracture of coated materials, *Reports in Mechanical Engineering*, 2(1), 2021, 6-22.
- [16] Kahn, L.F., Mitchell, A.D., Shear friction tests with high-strength concrete, *Structural Journal*, 99(1), 2002, 98-103.
- [17] Mansur, M., Vinayagam, T., Tan, K.-H., Shear transfer across a crack in reinforced high-strength concrete, *Journal of Materials in Civil Engineering*, 20(4), 2008, 294-302.
- [18] Kent, A., Harries, G.Z., Bahram, S., Toward an Improved Understanding of Shear-Friction Behavior, *ACI Structural Journal*, 109(6), 2012, 835-844.
- [19] Sneed, L.H., Krc, K., Wermager, S., Meinheit, D., Interface shear transfer of lightweight-aggregate concretes with different lightweight aggregates, *PCI Journal*, 61(2), 2016, 1-11.
- [20] Xiao, J., Li, Z., Li, J., Shear transfer across a crack in high-strength concrete after elevated temperatures, *Construction and Building Materials*, 71, 2014, 472-483.
- [21] Rahal, K.N., Khaleefi, A.L., Al-Sanee, A., An experimental investigation of shear-transfer strength of normal and high strength self compacting concrete, *Engineering Structures*, 109, 2016, 16-25.
- [22] Hertz, K.D., Concrete strength for fire safety design, *Magazine of Concrete Research*, 57(8), 2005, 445-453.
- [23] Ahmad, S., Bhargava, P., Chourasia, A., Shear transfer capacity of reinforced concrete exposed to fire, *IOP Conference Series: Earth and Environmental Science*, 140(1), 2018, 012146.
- [24] Hussein, H.H., Sargand, S.M., Khoury, I., Al-Jhayyish, A.K., Environment-Induced Behavior of Transverse Tie Bars in Adjacent Prestressed Box-Girder Bridges with Partial Depth Shear Keys, *Journal of Performance of Constructed Facilities*, 31(5), 2017, 04017074.
- [25] Ahmad, S., Bhargava, P., Chourasia, A., Direct shear failure in concrete joints exposed to elevated temperatures, *Structures*, 27, 2020, 1851-1859.
- [26] Ahmad, S., Bhargava, P., Chourasia, A., Usmani, A., Effect of elevated temperatures on the shear-friction behaviour of concrete: Experimental and analytical study, *Engineering Structures*, 225, 2020, 111305.
- [27] Zhang, W., Niu, R., Zhang, G., Wang, Y., Mechanical Properties of Shear Key in Composite Segment for Shield Tunnel under High Temperature Welding, *Journal of Materials in Civil Engineering*, 35(3), 2023, 04022474.
- [28] ANSYS ANSYS User's Manual Revision 15, ANSYS, Inc, 2021.
- [29] Kent, D.C., Park, R., Flexural members with confined concrete, *Journal of the Structural Division*, 97(7), 1971, 1969-1990.
- [30] ACI committee 318 Building Code Requirements for Structural Concrete (ACI 318-14): An ACI Standard; Commentary on Building Code Requirements for Structural Concrete (ACI 318R-14), *American Concrete Institute*, 2014.
- [31] Chang, Y.-F., Chen, Y.-H., Sheu, M.-S., Yao, G.C., Residual stress-strain relationship for concrete after exposure to high temperatures, *Cement and Concrete Research*, 36(10), 2006, 1999-2005.
- [32] Tao, Z., Wang, X.-Q., Uy, B., Stress-strain curves of structural and reinforcing steels after exposure to elevated temperatures, *Journal of Materials in Civil Engineering*, 25(9), 2013, 1306-1316.
- [33] Mattock, A.H., Li, W., Wang, T., Shear transfer in lightweight reinforced concrete, *PCI Journal*, 21(1), 1976, 20-39.

ORCID iD

Rajai Z. Al-Rousan  <https://orcid.org/0000-0001-6981-7420>

Bara'a R. Alnemrawi  <https://orcid.org/0000-0001-9097-7250>



© 2023 Shahid Chamran University of Ahvaz, Ahvaz, Iran. This article is an open access article distributed under the terms and conditions of the Creative Commons Attribution-NonCommercial 4.0 International (CC BY-NC 4.0 license) (<http://creativecommons.org/licenses/by-nc/4.0/>).

How to cite this article: Al-Rousan R.Z., Alnemrawi B.R. Prediction of Interface Shear Strength of Heat Damaged Shear-keys using Nonlinear Finite Element Analysis, *J. Appl. Comput. Mech.*, 9(4), 2023, 1000-1015.
<https://doi.org/10.22055/jacm.2023.42998.4000>

Publisher's Note Shahid Chamran University of Ahvaz remains neutral with regard to jurisdictional claims in published maps and institutional affiliations.

